RESEARCH ARTICLE

Investigation of Thermodynamic and Morphological Properties of Crystalline 4-HPG (4-hydroxyphenylglycine) Using Raman, PXRD and DTA/TGA

M. Fatih Ergin* 🆔

Department of Chemical Engineering, Engineering Faculty, Istanbul University- Cerrahpasa, Istanbul / Turkey

Abstract: This study focuses on the detailed physical characterization of 4-HPG, a significant impurity found in some of the most commonly prescribed β-lactam antibiotics worldwide. Various analytical techniques, including X-ray powder diffractometry, dynamic light scattering, scanning electron microscopy, Fourier-transform infrared, and Raman spectroscopy, were employed to characterize the properties of 4-HPG crystals. XRD analysis revealed the crystallinity and small crystallite sizes of 4-HPG particles, supported by DLS and SEM analyses. FT-IR and Raman spectroscopy results exhibited excellent agreement, providing insight into the structural characterization of 4-HPG. Thermal analysis revealed a two-stage degradation feature of 4-HPG. Overall, this study contributes to a better understanding of 4-HPG's structure and its impact on antibiotic stability.

1. INTRODUCTION

Today, studies on the physical characterization of active pharmaceutical ingredients (APIs) examine drug stability (1) in detail within formulation programs that encompass analytical tests (2) and the physical properties of the drug substance (3-7). Understanding the properties of APIs, as well as their impurities, is equally crucial for comprehending their effects on pharmaceutical structure. A sufficiently detailed physical framework of both the API and its impurities serves as a vital starting point in addressing undesirable crisis situations stemming from raw materials. Thermal analysis methods provide information on the material's physical characteristics depending on its temperature.

Combining thermal analysis (TG, DTA) (8) with electron microscopy (SEM), Raman and FT-IR spectroscopy, and X-ray powder diffractometry (XRD) offers a comprehensive view of the chemical and physical changes occurring in pharmaceuticals (9, 10).

An analog of tyrosine, an amino acid with intriguing photophysical activity in a peptide chain, is 4-hydroxyphenylglycine (4-HPG) (Figure 1) (11). Additionally, 4-hydroxyphenylglycine is one of the main components of Complestatin, a neuroprotective agent (12). Furthermore, surface-functionalized single-walled carbon nanotubes with azomethine ylide groups and fixed phenol structures are created using 4-HPG (13).

Figure 1: Molecular structure of 4-hydroxyphenylglycine.

Chiral amino acid derivatives, such as D(-)/L(+) - 4-Hydroxyphenylglycine, exhibit easy accessibility, multiple metal binding sites, and versatile binding modes, making them ideal candidates for forming compounds. Li et al. formed complexes with D/L -4-HPG, Pb(II), Cu(II), and Cd(II) metals, showcasing the structural diversity and potential of D/L-4-HPG in synthesizing coordination compounds with intriguing structures (14). HPG, known for its large specific surface area and strong cohesion strength with catalyst nanoparticles, was utilized alongside $Co_{0.85}Se$ in the electrochemical water cracking process in alkaline solution by Zhong et al (15). Mostaghasi et al. prepared Fe_3O_4-HPG-FA nanoparticles, demonstrating their

potential as efficient nanotheranostic devices for eliminating cancer cells (16). Liu et al. developed 3D HPG-supported high-performance $Pt/NiCo_2O_4$ for glycerol electrooxidation (17). He et al. synthesized Fe_3O_4/HPG-COOH nanoparticles and highlighted their effectiveness as an adsorbent to remove cationic dyes from water (18).

Moreover, 4-HPG is widely used as an acyl donor in the enzymatic synthesis of Amoxicillin trihydrate (AMCT), a cephalosporin-type β-lactam antibiotic (19, 20). However, regardless of the production method used (Figure 2), it is inevitable that 4-HPG will appear as an impurity along with the desired AMCT (21, 22).
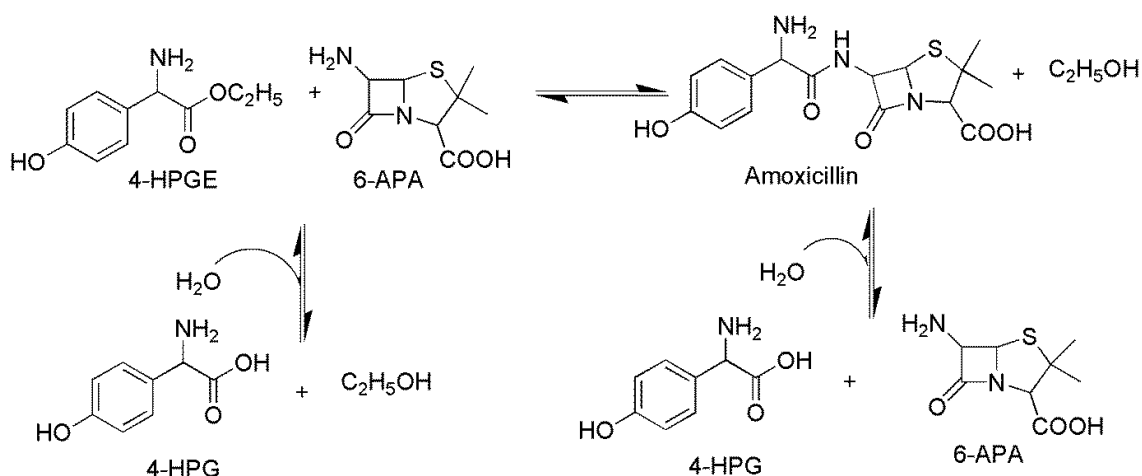
Figure 2: Enzymatic synthesis for the production of AMCT.

Impurities in β-lactam crystallization adversely affect nucleation and growth rate. Hence, considerable attention has been given in the literature to identifying and purifying impurity products of AMCT, especially 4-HPG (23-26). The quantitative measurement of organic and medicinal components, as well as completed goods and contaminants, is carried out using various methodologies (27-29). The presence of degradation products of AMCT, especially 4-HPG, reduces synthesis efficiency and affects downstream purification and separation processes. Therefore, detailed physical characterization of 4-HPG is essential to avoid adverse effects on the AMCT process. Ergin and Yasa developed a fast, simple, and specific UV-spectrophotometric method for determining 4-HPG and 6-APA (30). This study takes a step towards understanding the effects of 4-hydroxyphenylglycine (4-HPG), a significant impurity in some of the world's most commonly prescribed beta-lactam antibiotics such as amoxicillin trihydrate, by providing a comprehensive physical characterization. By shedding light on the role of 4-HPG in pharmaceutical products, enhancing quality control, and optimizing production efficiency, this research aims to illuminate the latest developments in the industry. It represents a stride forward in the pharmaceutical industry towards

producing safer, more effective, and more reliable medications.

2. EXPERIMENTAL SECTION

4-HPG purchased from Sigma Aldrich (USA) was of analytical purity and used without additional purification steps. The Milli-Q system (Millipore, USA) was employed to produce distilled water throughout the study. Hydrochloric acid and sodium hydroxide from Sigma-Aldrich were used to prepare 1.0 M HCl and 5.0 M NaOH solutions, respectively.

2.1. Crystallization
In this study, a pre-designed Büchner glass funnel was used to easily obtain crystals without losing them and to operate at the desired temperature (24, 30, 31). The temperature of the process was set to room temperature with a circulating water bath (VWR Science 1150) and the system was operated at the same temperature for 30 minutes. All solvents were kept at the specified temperature (room temperature) in the water bath during the process to stabilize the system. 5.0 g of 4-HPG and 100 mL of deionized water were added to the jacketed reactor and stirred at 300 rpm with a mechanical stirrer (Ika RW 16) for 5 min. Then, 1 M HCl was fed into a jacketed reactor at the same

temperature as the solution (pH: 1.9, about 45 mL HCl) until all 4-HPG was dissolved. The undissolved solids were eliminated using 0.45 m Whatman Nylon filter paper. The solution was then fed with 5 M NaOH solution until pH reaches 5.0 and then allowed to crystallize for 30 min. A pH meter was used to continuously monitor the pH of the HCl and NaOH stages (Fischer Scientific AE 150, USA). The crystals obtained were filtered using Whatman Nylon filter paper with a pore size of 0.2 m. The resulting crystal samples were gently removed and dried for use in the experiments (Figure 3).
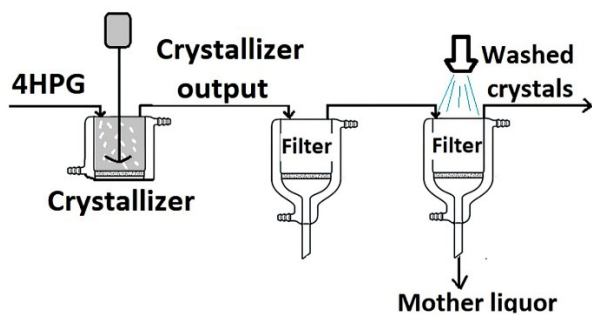
Figure 3: Schematic presentation of the 4-HPG crystallization process.

2.2. Thermogravimetric Analysis (TGA-DTG)

The thermal degradation behavior was analyzed using a Shimadzu DTG 60H instrument under airflow, with a heating rate of 10 °C min^{-1}, from room temperature to 800 °C in platinum crucibles.

The heating rate of 10 °C min^{-1} signifies how rapidly the temperature of the sample increases during the analysis. This parameter influences the rate of thermal degradation and provides insight into the stability of the material under investigation. A higher heating rate may accelerate the degradation process, whereas a lower rate allows for a more detailed observation of degradation behavior.

The analysis conducted under airflow indicates that continuous air circulation around the sample was maintained during heating. This airflow helps remove volatile degradation products and maintains consistent temperature conditions throughout the analysis. However, inert atmospheres such as nitrogen or argon were not preferred due to their potential impact on the degradation behavior of the sample.

Overall, the detailed parameters of thermal analysis, including heating rate, atmosphere conditions, and sample preparation, play a significant role in accurately characterizing the thermal degradation behavior of the material under investigation.

2.3. X-ray Diffraction (XRD)

The crystallographic structure analysis was performed using a Rigaku D/max-2200 X-ray diffractometer

equipped with CuKα radiation. The scan rate was set at 2θ = 0.01°/s over the angular range of 2° to 40°.

During XRD analysis, the sample preparation involved finely grinding the crystalline material to a powder form and uniformly spreading it onto a sample holder. The sample holder was then positioned in the X-ray beam path, and the diffraction pattern was recorded as the sample was rotated.

The obtained diffraction pattern consists of peaks corresponding to the crystal lattice planes of the material. The positions and intensities of these peaks provide information about the spacing between lattice planes and the arrangement of atoms in the crystal structure.

To analyze the data, the diffraction pattern is compared to standard reference patterns available in powder diffraction files (PDFs) from the International Centre of Diffraction Data (ICDD). By matching the observed peaks with those in the reference patterns, qualitative phase analysis can be performed to identify the crystalline phases present in the sample.

$$n\lambda = 2d \cdot \sin \theta \qquad \text{(Eq. 1)}$$

$$d = (0.94\lambda)/(\beta\cos\theta) \qquad \text{(Eq. 2)}$$

Crystallite sizes were estimated using the Scherrer equation (Equation 2), with d representing crystallite size, λ representing X-ray wavelength, β representing full-width at half maximum (FWHM), and θ representing the diffraction angle. The average d-spacing, d (Å), was calculated using Bragg's equation (Equation 1) (32). Crystallite size was calculated based on the peak (100).

2.4. Raman Spectrometer

A Raman spectrometer (Model Thermo DXR) with a spectral range of 3200–400 cm^{-1} was used for the analysis of 4-HPG. Ideal Raman conditions were determined as 532 nm, 10.0 mW, 10, 4.0 s, 2 and 50 m pinholes, respectively.

2.5. Fourier Transform Infrared Spectroscopy (FT-IR)

The FT-IR spectra of the samples synthesized in this study were recorded in the Thermo Nicolet 380 FT-IR brand spectrometer, in the range of 4000-400 cm^{-1}.

2.6. Particle Size Analysis

Particle sizes were determined using Dynamic Light Scattering (DLS) with a Brookhaven 90 Plus submicron particle size analyzer.

In DLS analysis, the sample, either a solution or dispersion, is illuminated with a monochromatic laser beam. This light is scattered by the particles in the sample. The DLS analyzer measures the properties of this scattering and calculates the particle size distribution using these data.

2.7. Scanning Electron Microscope (SEM)

Thermo Fisher Scientific's FEI FEG Quanta 250 scanning electron microscope (SEM) with energy-dispersive X-ray spectroscopy was used to analyze the microstructures of 4-HPG.

3. RESULTS AND DISCUSSION

3.1. Thermogravimetric Analysis

To date, only a limited number of studies have been conducted on the thermal behavior of amoxicillin in its pure form and in combination with specific excipients (31-33). Additionally, Bhattacharya et al. (1994) mentioned the determination of the melting point of HPG in their study on the synthesis of D-4-Hydroxyphenylglycine, but they did not provide any data or graphs regarding this (34). This study presents, for the first time, the Thermogravimetric Analysis (TGA) and Differential Thermal Analysis (DTA) spectra demonstrating the thermal properties of 4-hydroxyphenylglycine (4-HPG), a common impurity found in amoxicillin.

This study highlights the critical role of 4-HPG's thermal behavior as a prevalent impurity in amoxicillin.

Understanding the impact of 4-HPG's presence on the quality and stability of pharmaceutical products is crucial. The TGA and DTA spectra reveal a distinct two-step decomposition characteristic of 4-HPG. The structure of 4-HPG remains stable at room temperature, with no observed mass loss up to 210 °C, indicating its thermal stability until this temperature threshold. Upon reaching 210 °C, drug molecules acquire sufficient energy for orderly crystallization, followed by immediate melting and subsequent degradation of the molecules. The abrupt decrease in weight loss (~40%) observed in the temperature range of 210-255 °C is attributed to the elimination of the -COOH group (Table 1). Furthermore, a gradual reduction in mass is observed between 440 and 597 °C, accounting for approximately 54% of the mass, due to the decomposition of other groups remaining in the structure.

The examination of TGA and DTA spectra provides valuable information about the stability and decomposition properties of 4-HPG. The findings indicate that 4-HPG exhibits resistance to heat and possesses a stable structure. This understanding may contribute to discerning the potential impact of 4-HPG on the quality and stability of pharmaceutical products.

Table 1: Thermogravimetric data for compound 4-HPG.

Compound	Step	Temperature Range (°C)	Weight loss (%)	Residue
4-HPG	1st	210-255	39.51	60.49
	2nd	440-597	54.42	-

3.2. X-ray Diffraction (XRD) Analysis

Powder XRD (PXRD) was utilized to explore the crystal structure properties of 4-HPG. PXRD models of 4-HPG are depicted in Figure 5, presented for the first time in the literature, providing detailed insight into the crystal structures of 4-HPG. This analysis constitutes a novel contribution to the existing literature. Furthermore, comparative analysis with previous studies underscores the significance of our findings. Additionally, while Bathori et al. (2009) utilized 4-hydroxyphenylglycine to acquire D(-)-amino-(4-hydroxyphenyl) acetate crystals, subsequently analyzed through X-ray diffraction, our study expands upon this research by offering a comprehensive examination of 4-HPG's crystal structures (13).
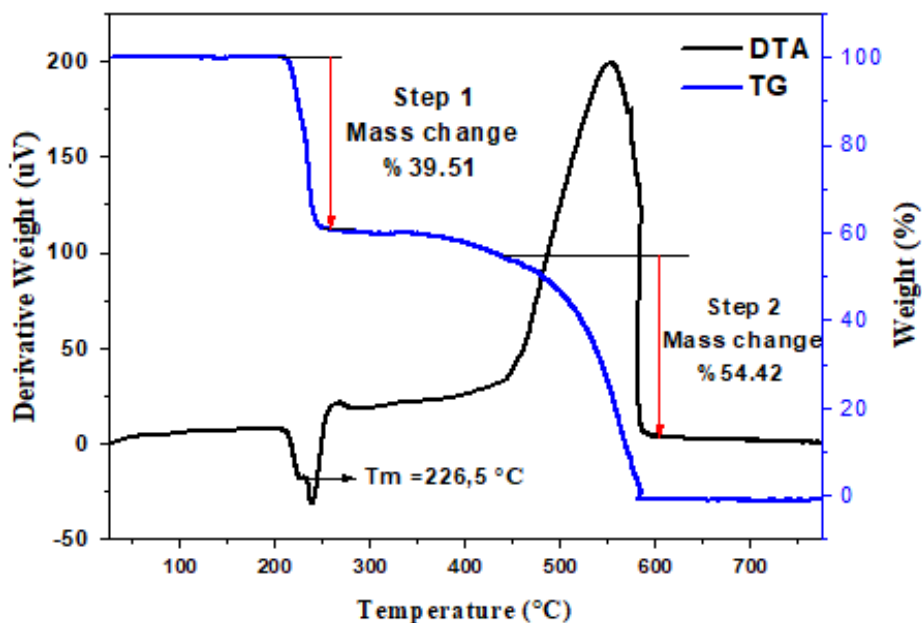
Figure 4: TGA-DTA graphics of the 4-hydroxyphenylglycine.

The highest intensity peak value of the 4-HPG particles was observed at 2θ: 20.51°, corresponding to the scattering from the (100) plane. Other peaks in the structure delineate the crystal structure of 4-HPG, with 2θ values of 20.51°, 27.50°, 35.66°, 40.07°, and 41.97° corresponding to crystalline (h k l) Miller indices (100), (101), (110), (111), and (012), respectively, indicative of the hexagonal phase 4-HPG crystals. 4-HPG exhibits relatively intense and sharp peaks with good crystallinity. The d-spacing values of 4-HPG were calculated in accordance with Bragg's equation and are detailed in Table 2, with a calculated value of 0.43 nm. Additionally, the intensity of XRD peaks of the sample clearly indicates the crystalline nature of 4-HPG particles, with broad diffraction peaks suggesting small crystallite sizes. The crystallite sizes of 4-HPG particles were determined to be approximately ~43 nm. Furthermore, it is noteworthy to mention that the crystal structure properties of 4-HPG serve as a significant source of information for researchers in the field.
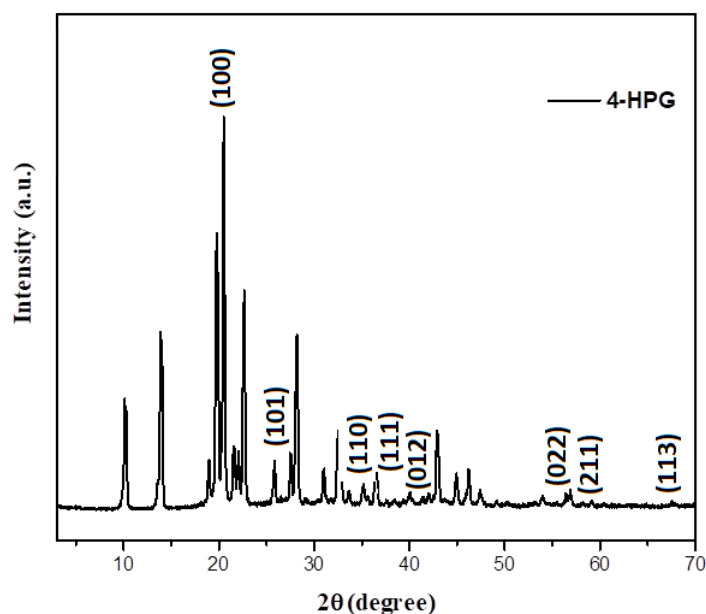
Figure 5: X-rays powder diffractograms of 4-HPG structure.

3.3. Fourier Transform Infrared Spectroscopy (FT-IR) and Raman Analysis

Figure 6 shows the characteristic FT-IR spectrum of 4-HPG crystals in detail. Between 3200 cm^{-1} and 2500 cm^{-1} and between 1700 cm^{-1} and 400 cm^{-1} wavenumbers,

variations in transmission spectroscopy data were noted. These results are in accordance with the amoxicillin literature (33, 35). It is also compatible with the graph given by Yokozeki et al. (1987) for d-4-hydroxyphenylglycine (36). Figure 7 shows the characteristic Raman spectrum of 4-HPG crystals. The Raman spectrum of 4-HPG was shown for the first time in the literature in this study and examined in detail. Thus, it will shed light on the work of many researchers.

O-H stretching of COOH, phenolic OH, and NH stretching vibrations cause an overlap of peaks in the wide band envelope between 2000 and 3500 cm^{-1}. Due to their shared characteristics, the N-H and O-H groups superimpose and were located at 3212 cm^{-1} in the FT-IR and 3192 cm^{-1} in the Raman spectrum. Asymmetric vibrations of C-H at 2967 cm^{-1} and C-H bond the of aromatic ring at 3061 cm^{-1} were also seen in FT-IR, and

at 3070 cm^{-1} and 2958 cm^{-1} in the Raman spectrum, respectively. Since amino acids exist in the form of zwitter ions, they contain amine and carboxylate salts in their structure. Ammonium ion was detected at 1605 cm^{-1} and 1523 cm^{-1} in FT-IR, and 1603 and 1523 cm^{-1} in Raman, respectively. COO^- stretching vibration is lower than the free acid group. It gives strong asymmetric peak at 1626 cm^{-1} and 1405 cm^{-1} in FT-IR, at 1626 cm^{-1} and 1405 cm^{-1} in Raman spectrum. The vibrations of the para-substituted benzoic ring produce peaks of high intensity at 847 cm^{-1} in FT-IR, at 868 cm^{-1} in Raman spectrum.

It is seen in Figure 8 that the FT-IR and Raman spectrum values support each other with great agreement. In addition, it is in harmony with the structure. Thus, they will shed light on the work of many researchers and may also be useful for the quantitative analysis of the phase composition of the pharmaceutical material (37).
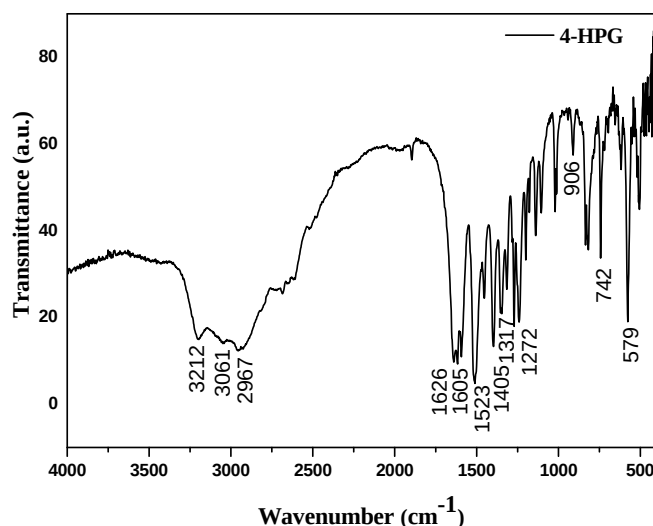
Figure 6: FT-IR spectra of 4-HPG structure.
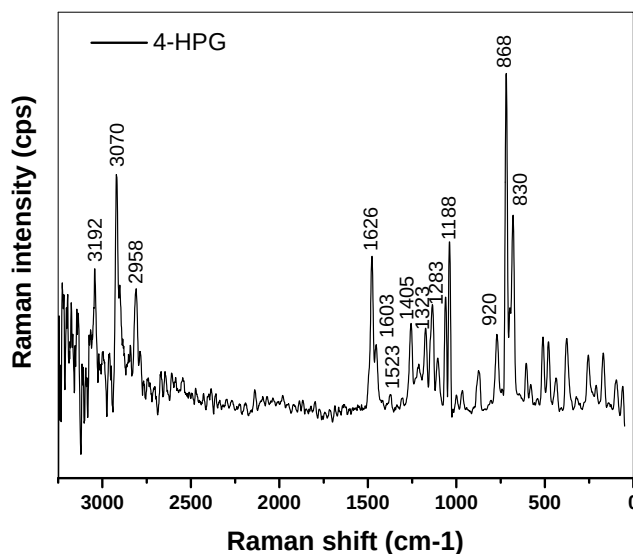
Figure 7: Raman spectra of 4-HPG.

Table 2: Peak search report of 4-HPG structure from X-rays powder pattern.

2-Theta	d-spacing (nm	Height	I%	Area	Area%	FWHM	Crystallite Sizes (nm)	Miller indices (h k l)
10.13	0.87	880	28.7	13183	34.4	0.254	34	
13.91	0.63	1410	46.0	24942	65.0	0.301	28	
18.17	0.48	23	0.7	271	0.7	0.205	44	
18.98	0.46	355	11.6	5263	13.7	0.252	34	
19.78	0.44	2098	68.4	33995	88.6	0.275	31	
20.51	0.43	3068	100.0	38358	100.0	0.213	43	(1 0 0)
21.56	0.41	397	12.9	5858	15.3	0.251	35	
22.07	0.40	392	12.8	6262	16.3	0.271	32	
22.66	0.39	1714	55.9	23906	62.3	0.237	37	
25.84	0.34	331	10.8	4563	11.9	0.234	38	
27.50	0.32	363	11.8	3923	10.2	0.184	53	(1 0 1)
28.20	0.31	1339	43.6	21732	56.7	0.276	31	
29.14	0.30	41	1.3	435	1.1	0.178	55	
31.05	0.28	274	8.9	4318	11.3	0.268	33	
32.52	0.27	573	18.7	12762	33.3	0.378	22	
33.62	0.26	95	3.1	1234	3.2	0.220	42	
35.22	0.25	144	4.7	2945	7.7	0.347	25	
35.66	0.25	54	1.8	1054	2.7	0.329	26	(1 1 0)
36.51	0.24	374	12.2	6197	16.2	0.281	31	
37.63	0.23	33	1.1	271	0.7	0.141	84	
38.52	0.23	43	1.4	494	1.3	0.193	50	
39.38	0.22	36	1.2	265	0.7	0.125	>100	
40.07	0.22	106	3.5	1824	4.8	0.292	30	(1 1 1)
41.37	0.21	43	1.4	363	0.9	0.142	84	
41.97	0.21	64	2.1	934	2.4	0.248	37	(0 1 2)
42.88	0.21	566	18.4	9106	23.7	0.274	33	
44.92	0.20	241	7.9	3648	9.5	0.257	36	
46.22	0.19	279	9.1	4050	10.6	0.247	38	
47.40	0.19	117	3.8	1990	5.2	0.291	31	
49.18	0.18	41	1.3	417	1.1	0.171	63	
50.18	0.18	31	1.0	629	1.6	0.342	26	
53.99	0.17	73	2.4	1345	3.5	0.314	29	
55.49	0.16	26	0.8	301	0.8	0.193	54	
56.40	0.16	100	3.3	1286	3.4	0.219	46	(0 2 2)
56.88	0.16	129	4.2	2468	6.4	0.326	29	
59.12	0.15	43	1.4	533	1.4	0.212	49	(2 1 1)
67.51	0.13	41	1.3	907	2.4	0.372	26	(1 1 3)

3.4. Morphology and The Particular Size of 4-HPG

Many studies in the literature have focused on examining the SEM image of pure AMCT or its mixtures. The SEM results obtained revealed the long acicular rectangular prismatic structure of AMCT crystals (38). Although 4-HPG is one of the most critical impurities of AMCT mentioned in the USP (39), SEM images showing 4-HPG are still not available in the literature. This study is very important as it is the first to use SEM images to reveal the surface and morphology of 4-HPG crystals in detail (Figure 9a, 9b, and 9c). It also enabled the identification of 4-HPG present as an impurity in the AMCT crystal lattice (Figure 9d).

In SEM images and DLS analysis of 4-HPG crystals, it was observed that the average particle size is between 500 nm and 1500 nm (Figure 10), rectangular prisms, and sharp-edged structures with regular geometric shapes. In addition, it was determined that the particles of 4-HPG were smaller than the crystals of amoxicillin, which were impurities.
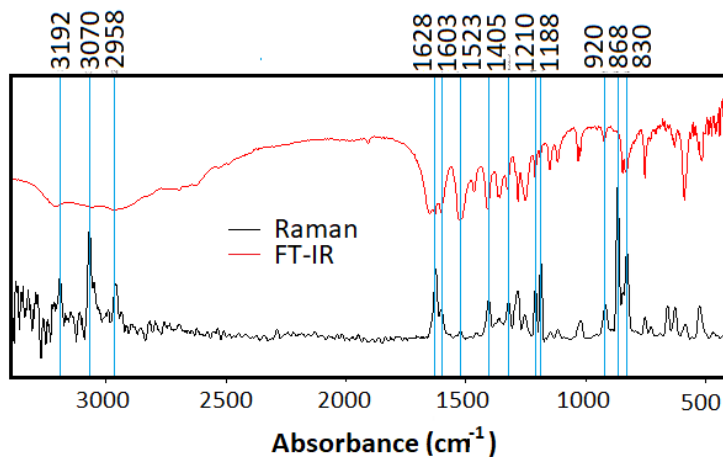
Figure 8: Comparison of FT-IR and Raman spectra.
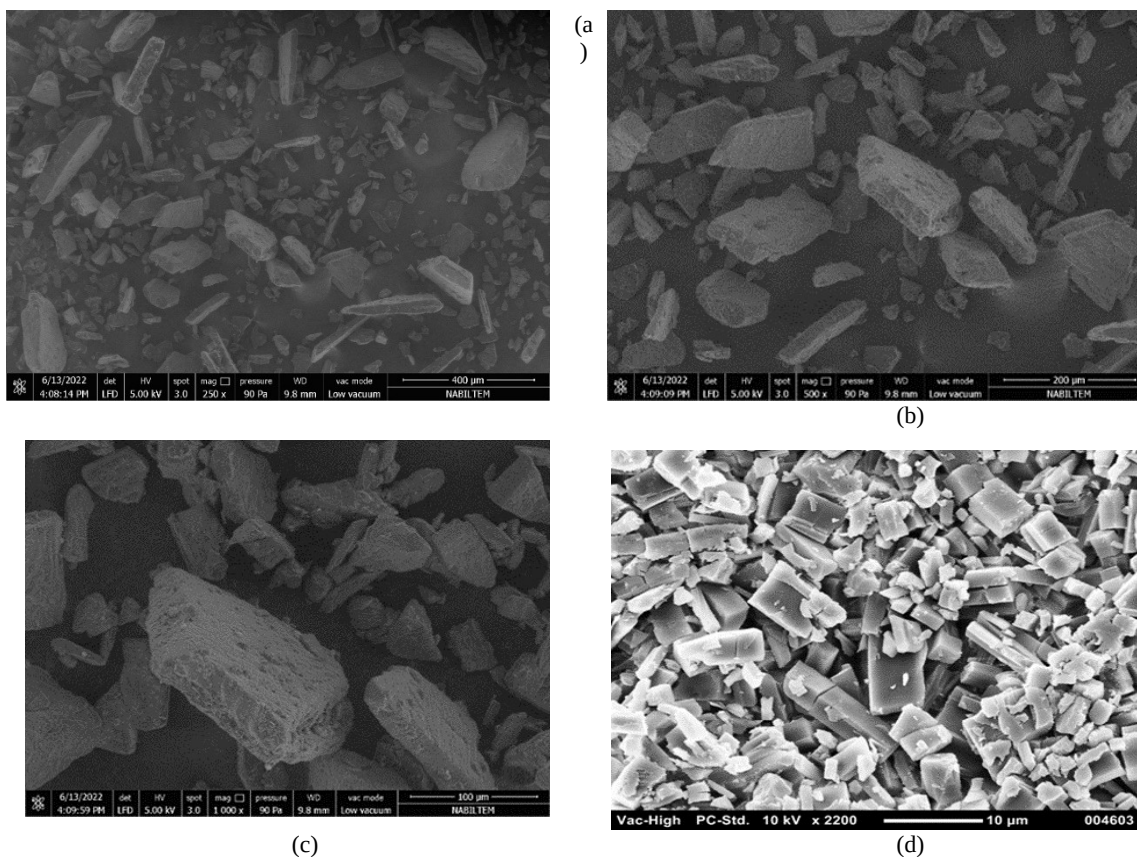
Figure 9: a,b,c) SEM images of 4-HPG and d) AMCT with impurities.
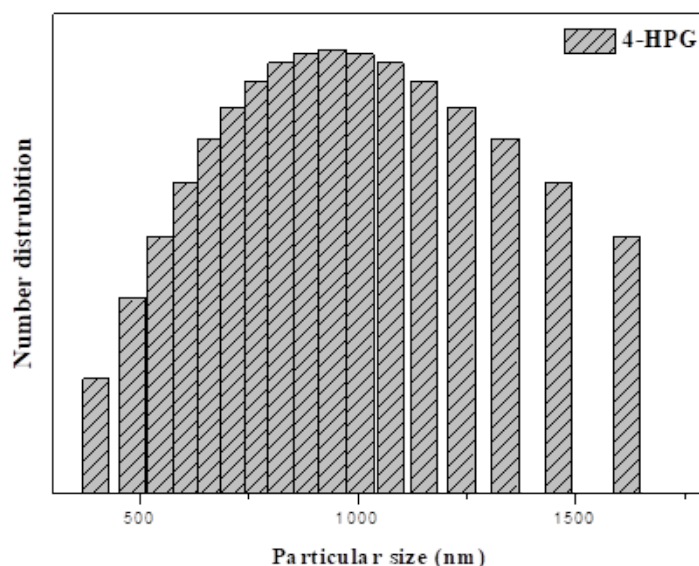
Figure 10: The particle size of 4-HPG crystals.

4. CONCLUSION

In an environment where competition is always intense in the pharmaceutical industry, one of the most important questions to address is how to achieve high yield rates and ensure product quality without compromising it. The fundamental solution to this issue, particularly in obtaining a pure product, lies in fully identifying and eliminating impurities that degrade quality. This study focuses on the detailed thermal, morphological, and physical characterization of 4-HPG, a significant impurity found in some of the most commonly prescribed β-lactam antibiotics worldwide, such as Amoxicillin, amoxicillin salt, amoxicillin trihydrate, cefadroxil, cefoperazone, cephalosporin, and cephalosporin hydroxylamine.

The study has helped us better understand the potential effects of 4-HPG on industrial applications and the quality of pharmaceutical products. Thermal analysis results have provided important insights into the thermal resistance and stability of 4-HPG, which can affect the stability and shelf life of relevant pharmaceutical products. XRD analysis has thoroughly revealed the structural properties of 4-HPG crystals, and this information can assist in understanding the crystal structures of relevant products and optimizing production processes. FT-IR and Raman spectroscopy shed light on the molecular structure of 4-HPG and provide a basis for understanding the potential effects of impurities on the quality of pharmaceutical products. These findings can play a significant role in the industrial applications of 4-HPG and the development of pharmaceutical products.

Given that 4-HPG significantly affects the shelf life and stability of antibiotics in which it is present, it is crucial to define its structure in detail.

7. REFERENCES

1.   McGinity JW. Drug Stability: Principles and Practices. Journal of Pharmaceutical Sciences. 1991;80(1):98.

2.   Ohannesian L, Streeter A. Handbook of pharmaceutical analysis: CRC Press; 2001.

3.   Fiese E, Hagen T. Preformulation In: The Theory and Practice of Industrial Pharmacy. Lachman L, Lieberman HA, Kanig JL. Varghese Publishing House; 1990.

4.   Wadke DA, Serajuddin AT, Jacobson H. Preformulation testing. Pharmaceutical dosage forms: Tablets. 1989;1:1-73.

5.   Carstensen JT. Pharmaceutical preformulation: crc Press; 1998.

6.   Gibson M. Pharmaceutical preformulation and formulation. Drugs the pharmaceutical sciences. 2001;199:199.

7.   Adeyeye MC, Brittain H. Drug-excipient interaction occurrences during solid dosage form development. THE PHARMACEUTICAL SCIENCES. 2008;178:357.

8.   Leite RS, Macedo RO, Torres SM, Batista CCN, Baltazar LO, Neto SL, et al. Evaluation of thermal stability and parameters of dissolution of nifedipine crystals. Journal of thermal analysis calorimetry. 2013;111(3):2117-23.

9.   Kocevska S, Maggioni GM, Crouse SH, Prasad R, Rousseau RW, Grover MA. Effect of ion interactions on the Raman spectrum of NO3−: Toward monitoring of low-activity nuclear waste at Hanford. Chemical Engineering Research Design. 2022;181:173-94.

10.   Lagerman CE, Grover MA, Rousseau RW, Bommarius AS. Reactor Design and Optimization of α-Amino Ester Hydrolase-Catalyzed Synthesis of Cephalexin. Frontiers in Bioengineering Biotechnology. 2022;10.

11.   Wiesław W, Krystyna S, Cezary C, Leszek Ł, Alicja M. Photophysical properties of (p-hydroxy) phenylglycine. Journal

of Photochemistry Photobiology A: Chemistry. 1997;102(2-3):189-95.

12. Kaneko I, Fearon DT, Austen K. Inhibition of the alternative pathway of human complement in vitro by a natural microbial product, complestatin. Journal of immunology. 1980;124(3):1194-8.

13. Báthori NB, Bourne SA. Crystal Structure of D (−)-amino-(4-hydroxyphenyl) acetate, the Zwitter Ionic Form of Biologically Active D (−)-4-hydroxyphenylglycine. Journal of Chemical Crystallography. 2009;39:539-43.

14. Li S, Cao M, Li Y, Yang J, Zhao M, Song H. Three pairs of Pb (II), Cd (II) and Cu (II) enantiomeric coordination compounds based on D-(−)-and L-(+)-4-Hydroxyphenylglycine: Synthesis, structures and properties. Journal of Molecular Structure. 2022;1255:132451.

15. Zhong Q-S, Xia W-Y, Liu B-C, Xu C-W, Li N. Co0. 85Se on three-dimensional hierarchical porous graphene-like carbon for highly effective oxygen evolution reaction. International Journal of Hydrogen Energy. 2019;44(21):10182-9.

16. Mostaghasi E, Zarepour A, Zarrabi A. Folic acid armed Fe3O4-HPG nanoparticles as a safe nano vehicle for biomedical theranostics. Journal of the Taiwan Institute of Chemical Engineers. 2018;82:33-41.

17. Liu B-C, Chen S-L, Ling X-Y, Li Q-X, Xu C-W, Liu Z-L. High activity of NiCo 2 O 4 promoted Pt on three-dimensional graphene-like carbon for glycerol electrooxidation in an alkaline medium. RSC advances. 2020;10(41):24705-11.

18. He Y, Cheng Z, Qin Y, Xu B, Ning L, Zhou L. Facile synthesis and functionalization of hyperbranched polyglycerol capped magnetic Fe3O4 nanoparticles for efficient dye removal. Materials Letters. 2015;151:100-3.

19. Kosmidis J, Williams J, Andrews J, Goodall J, Geddes A. Amoxycillin-pharmacology, bacteriology and clinical studies. Brit J Clin Practice. 1972;26(7):341-6.

20. Chen C-X, Wu Q, Liu B-K, Lv D-S, Lin X-F. Anhydrous tert-pentanol as a novel media for the efficient enzymatic synthesis of amoxicillin. Enzyme microbial technology. 2008;42(7):601-7.

21. Youshko MI, Moody HM, Bukhanov AL, Boosten WH, Švedas VK. Penicillin acylase-catalyzed synthesis of β-lactam antibiotics in highly condensed aqueous systems: Beneficial impact of kinetic substrate supersaturation: Biotechnology bioengineering. 2004;85(3):323-9.

22. Giron D, Goldbronn C, Mutz M, Pfeffer S, Piechon P, Schwab P. Solid state characterizations of pharmaceutical hydrates. Journal of thermal analysis calorimetry. 2002;68:453-65.

23. Ergin M. Purification of amoxicillin trihydrate in the presence of degradation products by different washing methods. CrystEngComm. 2021;23(46):8121-30.

24. ERGİN M. Yıkama Metodu Kullanılarak Saflaştırılan Amoksisilin Trihidratın Taguchi Yöntemi ile Optimizasyonu. Journal of the Institute of Science Technology. 2022;12(2):933-45.

25. Hsi KH, Kenny M, Simi A, Myerson AS. Purification of structurally similar compounds by the formation of impurity co-former complexes in solution. Crystal growth design. 2013;13(4):1577-82.

26. Hsi KHY, Concepcion AJ, Kenny M, Magzoub AA, Myerson AS. Purification of amoxicillin trihydrate by impurity-coformer complexation in solution. CrystEngComm. 2013;15(34):6776-81.

27. YAŞA H. Synthesis, characterization, and evaluation of antioxidant activity of new γ-and δ-imino esters. Turkish Journal of Chemistry. 2018;42(4):1105-12.

28. Onar HÇ, Vardar BA. Synthesis and antioxidant activity of novel 8-formyl-4-substitued coumarins. Bulletin of the Chemical Society of Ethiopia. 2018;32(1):175-8.

29. YAŞA H, Ergin MF, ERGİN A, ALKAN G. Importance of inert gases for chemical transportation. Proceedings Book. 2016:825.

30. Ergin M, Yasa H. Determination of amoxicillin trihydrate impurities 4-HPG and 6-APA by means of ultraviolet spectroscopy. Methods Applications in Fluorescence. 2022.

31. Celik Onar H, Ergin MF, Yasa H. Investigating the Role of Citric Acid as a Natural Acid on the Crystallization of Amoxicillin Trihydrate. ACS Omega. 2023;8(39):36344-54.

32. Nugrahani I, Asyarie S, Soewandhi SN, Ibrahim S. Solid state interaction between amoxicillin trihydrate and potassium Clavulanate. Malays J Pharm Sci. 2007;5(1):45-57.

33. Bisson-Boutelliez C, Fontanay S, Finance C, Kedzierewicz F. Preparation and physicochemical characterization of amoxicillin β-cyclodextrin complexes. Aaps Pharmscitech. 2010;11:574-81.

34. Bhattacharya A, Araullo-Mcadams C, Meier MB. Crystallization induced asymmetric transformation: synthesis of Dp-hydroxyphenylglycine. Synthetic communications. 1994;24(17):2449-59.

35. Fogazzi GB, Cantu M, Saglimbeni L, Daudon M. Amoxycillin, a rare but possible cause of crystalluria. Nephrology Dialysis Transplantation. 2003;18(1):212-4.

36. Yokozeki K, Nakamori S, Eguchi C, Yamada K, Mitsugi K. Screening of Microorganisms Producing d-p-Hydroxyphenyl-glycine from Dl-5-(-Hydroxyphenyty) hydantoin. Agricultural biological chemistry. 1987;51(2):355-62.

37. Bhat SA, Ahmad SJJoMS. FTIR, FT-Raman and UV–Vis spectral studies of d-tyrosine molecule. 2016;1105:169-77.

38. Feng S, Shan N, Carpenter KJ. Crystallization of amoxicillin trihydrate in the presence of degradation products. Organic process research development. 2006;10(6):1212-8.

39. Pharmacopeia U. USP 39-NF34. The United States Pharmacopeial. 2016.